Nanotechnology

PURPOSE-LED PUBLISHING™

PAPER

Porous polyvinyl alcohol/graphene oxide composite film for strain sensing and energy-storage applications

To cite this article: Xu Cui *et al* 2022 *Nanotechnology* **33** 415701

View the article online for updates and enhancements.

You may also like

- Preface
- The effect of the 2D internal strain state on the critical current in GdBCO coated conductors
Michinaka Sugano, Shutaro Machiya, Hidetoshi Oguro et al.
- *(Invited)* Tunable Large-Scale Compressive Strain Sensor Based on Carbon Nanotubes/PDMS Foam Composites By Additive Manufacturing
Linh Le, Junjun Ding, Chao Liu et al.

This content was downloaded from IP address 87.255.216.108 on 26/08/2025 at 12:55

IOP Publishing Nanotechnology
Nanotechnology 33 (2022) 415701 (14pp) https://doi.org/10.1088/1361-6528/ac7b35

Porous polyvinyl alcohol/graphene oxide composite film for strain sensing and energy-storage applications

Xu Cui[1], Jia Guo[1], Sherif Araby[2,3,*], Fethi Abbassi[4], Chunyan Zhang[1], Abdullatif Lacina Diaby[5] and Qingshi Meng[1,6,*]

[1] College of Civil Aviation, Shenyang Aerospace University, Shenyang 110136, People's Republic of China
[2] Department of Mechanical and Aerospace Engineering, Nazarbayev University, Nur-Sultan, 010000, Kazakhstan
[3] Department of Mechanical Engineering, Faculty of Engineering, Benha University, Benha, Egypt
[4] College of Engineering and Technology, American University of the Middle East, Kuwait
[5] UniSA Online (STEM), University of South Australia, SA 5000, Australia
[6] College of Aerospace Engineering, Shenyang Aerospace University, Shenyang 110136, People's Republic of China

E-mail: Sherif.Gouda@nu.edu.kz and mengqingshi@hotmail.com

Received 21 March 2022, revised 31 May 2022
Accepted for publication 22 June 2022
Published 19 July 2022

Abstract

In this study, a flexible porous polyvinyl alcohol (PVA)/graphene oxide (GO) composite film was developed and tested for flexible strain sensing and energy-storage applications. Morphology and mechanical properties were studied; tensile strength and Young's modulus increased by 225% and 86.88%, respectively, at 0.5 wt% GO. The PVA/GO film possesses exceptional sensing ability to various mechanical strains, such as tension, compression, bending, and torsion. For example, the gauge factor of the PVA/GO film as a tensile-strain sensor was measured as 2.46 (246%). Under compression loads, the PVA/GO composite film showed piezoresistive and capacitive strain-sensing characteristics. Under 5 kPa of compression load, the relative resistance increased by 81% with a 100 msec response time; the relative capacitance increased by 160% with a 120 msec response time. The PVA/GO strain sensor exhibited high durability and reliability over 20×10^3 cycles of tensile strain and bending at 3.33 Hz. Moreover, the PVA/GO composite film showed good electrochemical properties due to its porous structure; the maximum capacitance was 124.7 F g^{-1} at 0.5 wt% GO. After 20×10^3 charging–discharging cycles, the capacitance retention rate was 94.45%, representing high stable capacitance performance. The results show that electrically conductive porous PVA nanocomposite films are promising candidates for strain sensing and energy-storage devices.

Keywords: graphene oxide, porous structure, polyvinyl alcohol, strain sensor, specific capacitance

1. Introduction

In recent years, research on modern flexible electronic applications has focused on emerging lightweight and flexible electronics [1–3]. Electrically conductive flexible composite films possess promising prospects in energy storage, flexible displays, e-skins in wearable devices, and strain sensors [4–8]. Chuanhui *et al* [9] introduced an electrically conductive elastomer film based on carboxylic styrene-butadiene rubber, citric acid, and silver nitrate. The synthesized film showed robustness in mechanical properties, high flexibility, and conductivity; it also showed high sensitivity to humidity.

* Authors to whom any correspondence should be addressed.

 © 2022 IOP Publishing Ltd

In another study, polyvinyl alcohol-polyacrylamide/Zn/ethylene glycol (PPEG) organohydrogel-based ionic skin was found to be flexible, anti-freezing, and moist with good sensing performances; its signal response time was 0.23 s even at −50 °C [10].

Although the abovementioned studies involved conductive flexible composite films, few reports pay attention to porous conductive flexible composite films. Porous electrically conductive polymer nanocomposites feature a large internal surface area, high flexibility, and high specific strength, endowing them with various functionalities including electrochemical, electromechanical, and adsorption properties [11–14]. With the rapid development of modern technology, the demand for porous flexible conductive composite films with electrochemical and electromechanical properties is increasing. A three-dimensional (3D) porous MXene ($Ti_3C_2T_x$)/polyvinyl alcohol hydrogel showed excellent capacitive strain-sensing properties with up to 200% low hysteresis and a sensitivity of ≈0.40 [15]. Porous graphene/iron pentacarbonyl films showed high electromagnetic radiation attenuation [16]. Molla-Abbasi *et al* [17] fabricated a novel gas sensor using polymethyl methacrylate/multiwalled carbon nanotubes with a porous structure composite with high responsiveness to a range of organic vapors. Han *et al* [18] fabricated a novel hydrogel electrolyte using sodium alginate/Zn with a porous structure composite and reported good results in improving the energy density of the supercapacitor. Yu *et al* [19] prepared porous carbon nanotubes/polyvinylidene fluoride composite films with excellent hydrophobic and oil-philic properties; their results show promising environmental applications such as in oil separation. Elsewhere [20], a flexible supercapacitor composite based on porous polypyrrole (PPy) and a zeolitic imidazolate framework (ZIF) was developed. The specific capacitance of the composite was found to have increased from 99.2 F g^{-1} for pristine ZIF-67 to 597.6 F g^{-1} for ZIF−PPy networks, highlighting the significance of the latter.

With the continuous development of materials, science, and general awareness of environmental protection, biodegradable materials are being favored by scholars and modern industry [21–24]. Polyvinyl alcohol (PVA) is a green and biodegradable thermoplastic with excellent mechanical and chemical features. It decomposes into carbon dioxide and water without causing environmental pollution. PVA is highly soluble in water and has excellent film-forming properties. Its surface contains a large number of hydroxyl groups, therefore it can form strong intramolecular and intermolecular hydrogen bonds, endowing it with high tensile strength and excellent acid and alkali corrosion resistance [25–27]. However, PVA is inherently a nonconductive material, which hampers its application in advanced technologies such as wearable electronic devices and humanoid robots where biodegradable material is highly recommended. Adding functional nanofillers into polymers resulted in polymeric composites with multifunctionalities such as a thermally and electrically conductive polymer; yet the host polymer does not lose its inherent features, such as high flexibility and processability. Carbon-based nanomaterials such as carbon nanotubes and graphene possess excellent electrical and thermal conductivity, are light weight, have an outstanding surface area, and have superb mechanical properties [28–32]. Therefore, since PVA is a biodegradable polymer, we advocate using graphene to enhance the mechanical and functional properties of PVA.

Previous studies have worked on the addition of graphene oxide (GO) to PVA, demonstrating high mechanical properties as well as functional properties such as dielectric resistance [33–37]. For example, Yan *et al* [23] posited that GO improved the mechanical, thermal, and tribological properties of PVA; compared to pure PVA, the elastic modulus and hardness of 0.5 wt% PVA/GO were notably increased by 122.8% and 64.5%, respectively. The maximum decomposition temperature was increased by 68.4 °C at 0.5 wt% GO. Guo *et al* [36] prepared PVA/GO composites with high chemical resistance in harsh environments such as strong acid, strong alkali, and high-concentration brine. Boron-cross-linked GO/PVA hydrogels possessed high mechanical properties upon adding a low content of GO; at 0.1 wt% GO, the tensile strength increased 144% over B-PVA hydrogels [33]. Also, the compression and shear strength of the hydrogel increased by 26% and 35%, respectively. Kim *et al* [38] improved the thermal conductivity of PVA by 99.5%, with a maximum of 0.8 $Wm^{-1}K^{-1}$ at 4 wt% of GO. Despite the published studies on PVA composites, there are few reports on the application of PVA composite films in flexible electronic devices such as sensors and supercapacitors. In addition, the preparation and investigation of porous PVA/graphene has scarcely been reported.

In the current study, highly flexible porous PVA/GO composite films with multifunctionality for electromechanical (strain sensors) and electrochemical (supercapacitor electrodes) are reported. The morphology of GO and the porous structure of the PVA/GO composite films were investigated by transmission and scanning electron microscopies. The mechanical properties, sensing properties, water resistance, chemical resistance, and capacitance of the PVA/GO nanocomposite were investigated. Being a green polymer, the PVA/GO composites possess great potential in green energy harvesting devices and biocompatible wearable devices.

2. Experimental methods

2.1. Materials

Graphite powder was purchased from Qingdao Huatai Lubrication and Sealing Technology Co., Ltd. (China). Potassium permanganate was procured from Sinopharm Chemical Reagent Co., Ltd. (China). Phosphoric acid and concentrated sulfuric acid (98%) were obtained from Tianjin Beichen Founder Reagent Factory (China). PVA was provided by Shanghai Chenqi Chemical Technology Co., Ltd. (China). Glutaric dialdehyde (2%) was bought from Jiangsu Kangba Biological Engineering Co., Ltd. (China). All chemicals were used as received.

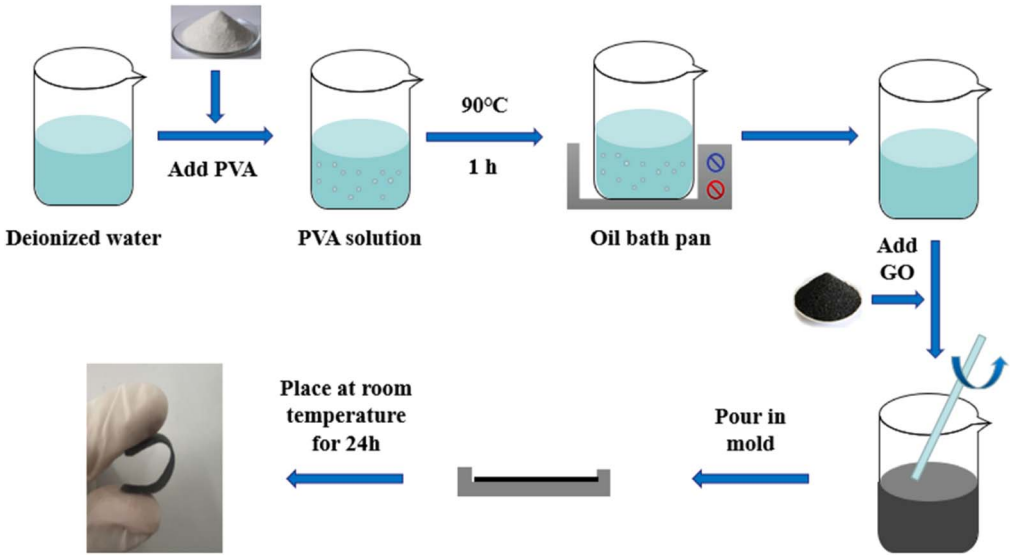

Figure 1. The fabrication of the flexible porous PVA/GO composite film.

2.2. Fabrication of GO and its porous PVA composite films

The modified Hummers method was applied to prepare the GO [39–41]. In a typical process of synthesis: (i) 6 g of concentrated sulfuric acid was slowly added into a mixture of 30 g phosphoric acid and 0.4 g potassium permanganate; the rate of addition was controlled to prevent the rapid rise in temperature of the suspension; it should be less than 20 °C. (ii) 0.1 g of graphite powder was added to the solution and magnetically stirred for 1 h. (iii) 200 ml of deionized water was added. The mixture was washed two times using deionized water, centrifuged, and collected. Finally, the collected paste was dispersed in 100 ml of acetone, centrifuged, and then collected. The collected paste was dried at 80 °C overnight. The end product was GO sheets.

The PVA/GO films were synthesized using a solution-casting method. Figure 1 shows the preparation process of the films; the procedures are as follows: (i) 4 g of PVA powder was dissolved in 40 ml of deionized water in an oil bath at 90 °C for 2 h; (ii) a predetermined weight of GO was added into the mixture; (iii) after the mixture had cooled to room temperature, 1 ml glutaric dialdehyde was added; (iv) the solution was then cast into a polytetrafluoroethylene (PTFE) mold; and (v) the PTFE mold with the cast was leveled and stored for 24 h at a constant temperature (25 °C), after which the PVA/GO composite film was peeled off.

2.3. Measurements

The morphology of GO was studied by high-power transmission electron microscopy (TEM; JEM-2100, JEL, Japan, 200 kV). The sample was prepared by dispersing GO into acetone using an ultrasonication bath; the process was repeated until a concentration of 0.0005 wt% GO was reached. Ten drops from the suspension were collected on 200-mesh copper grids and dried at 70 °C in a fan oven. The morphology of the PVA/GO composite was observed using scanning electron microscopy (SEM) at 5 kV (using an SU8010, HITACHI, Japan). Mechanical properties, including tensile strength, Young's modulus, and elongation at break, were determined using a universal tensile testing machine (GX-SF001, Shenzhen Shared Instrument Equipment Co. LTD., China). The crosshead speed was set at 2 mm min^{-1}; the tensile test was conducted at room temperature (25 °C). The test was replicated at least three times for each fraction of GO.

A FLUKE 2638 A data-acquisition system was used to investigate the electromechanical performance of the PVA/GO composite films. The electrical resistance was recorded using the acquisition system under different mechanical loads including tension, compression, bending, and torsion (twisting). In the course of testing, the sample was connected to the FLUKE data-acquisition system using copper wires and silver paste through which the change in resistance of the PVA/GO composite was recorded. The test conditions were set at a current source of 100 μA and a potential of 12 V. The gauge factor was calculated from equation (1):

$$GF = \frac{d(\Delta R/R_0)}{d\varepsilon}, \tag{1}$$

where ε is the mechanical strain applied to the sensor, and $\Delta R = R - R_0$, where R_0 and R are, respectively, the resistance of the sensor at the neutral state (no strain) and after the deformation.

Furthermore, fatigue tests were carried out on the same tensile machine within strain ranges of 0%–10% and 0%–50% at a frequency of 3.33 Hz. The test was run for 20 × 103 cycles. Furthermore, cyclic bending tests were carried out on 0.5 wt% PVA/GO composite film within an angle range 0°–45° and 0°–90° under a frequency of 3.33 Hz. During the fatigue test, the resistance of the sample was monitored by the FLUKE data-acquisition device.

Swelling resistance was assessed by a water-absorption method at room temperature. Water absorption of the films was evaluated by weighing. The sample was a square 20 mm in length. The sample was dried at 80 °C for 6 h to completely remove residual moisture. The initial mass of the sample was

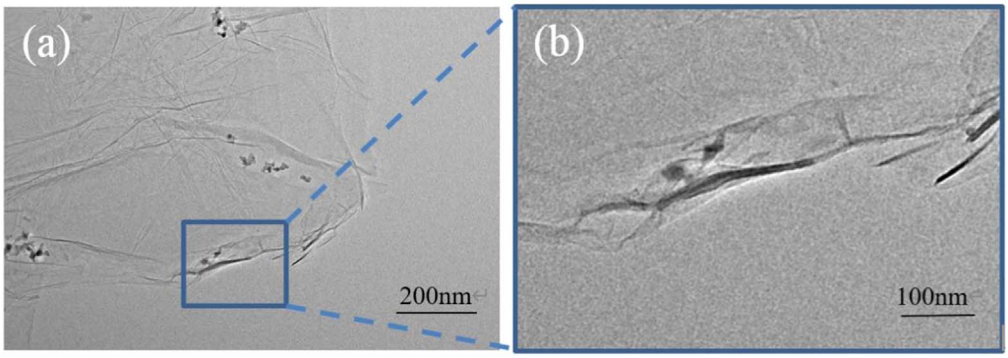

Figure 2. TEM micrographs of GO platelets.

weighed as W_o. Then, the sample was soaked in deionized water for 25 h until swelling saturation was reached. Finally, the sample was wiped carefully with a paper towel and weighed as W_f. The water was refreshed every 4 h. The percentages of water absorption were calculated using equation (2):

$$Water\ absorption(\%) = 100 \times \frac{W_f\text{-}W_0}{W_0}, \qquad (2)$$

where all variables have their usual meaning. For each point of measurement, three samples were used to obtain the average.

An electrochemical workstation (CHI660E B19038, Chenhua Instrument CO., Shanghai, China) was used to study the capacitive properties of the PVA/GO composite film. A LANHE battery-test system (Wuhan Ladian Electronics Co., Ltd. Ct 3001a1u) was used to study the cyclic charge–discharge performance of the composite film. The electrochemical parameters were tested and calculated according to previous work [42].

3. Results and discussion

3.1. Morphology of GO

The morphology of GO was observed by TEM, as presented in figure 2. The TEM image shows that the GO sheets had a thin sheet-like structure with a thickness at the nanoscale. There are a few stacking folds and wrinkles due to the distortions from the high fraction of sp^3 C–O bonds and oxidations by strong acids [43]. A similar morphology was reported in previous studies [44].

3.2. Morphology of the PVA/GO film

The morphology of the PVA/GO composite films was observed by a scanning electron microscope and their micrographs are shown in figure 3 at different contents of GO. In general, the SEM micrographs showed a porous microstructure for neat PVA and its GO nanocomposites. Figures 3(a1)–(a3) present a connected pores and network structure of neat PVA film; when a selected area is magnified in figure 3(a3), it is observed that the surface of PVA is smooth. Figures 3(b1)–(b3) display micrographs of the PVA composite film at 0.25 wt% GO; with the addition of GO, the porosity percentage decreases, as shown in figure 3(b1) in comparison with figure 3(a1). Also, adding GO increases the surface roughness of the pore surface. The microstructure of PVA/GO retains less porosity with thicker pore walls and higher surface roughness with the increase of GO content, as presented in figures 3(c1)–(c3) at 0.5 wt% GO and figures 3(d1)–(d4) at 0.75 wt% GO. Figure 3(d4) is a high-magnified image from a selected surface area of 0.75 wt% GO; it shows a paramount surface roughness of PVA/GO at 0.75 wt%. Therefore, figures 3(b1)–(b3), (c1)–(c3), and (d1)–(d4)) conclude that, the more GO wt%, the less porosity and the rougher the surface area. Consequently, although the SEM micrographs do not directly show GO sheets on the surface of PVA pores, the only reason for having a rough surface on the PVA is that the GO sheets precipitate and embed into the porous structure during the synthesis process. This confirms the effect of GO in strengthening the microstructure of the PVA's pores. Also, it means that GO plates at the pore's walls can form a global electrically conductive network within the PVA matrix and thus the composite is able to respond to mechanical strains, provided that it has a conductive network.

Further analysis on the microstructure of the PVA/GO composite films was conducted by ImageJ software to quantitatively study the pore size distribution and porosity percentage, as shown in figures 4(a)–(f). Generally, the pore diameter and porosity percentage decrease with the addition of GO, as shown in figures 4(e) and (f). Neat PVA possesses an average pore diameter of ∼100 μm; the pose size distribution is scattered between a small dimeter range (25–75 μm) and a large diameter range (125–275 μm), as shown in figure 4(a). Upon adding GO sheets, the percentage of small-diameter pores increases. For example, the average pore size of the PVA/GO composite at 0.5 wt% is 88 μm and ∼62% of the detected pores were in the range of (25–75 μm). At 0.75 wt%, 80% of the detected pores were at a diameter size of less than 125 μm and almost no pores at 225 or 275 μm. The porosity percentages of neat PVA and its GO composites were in line with pore size diameter; the porosity of neat PVA is ∼34.39%; it decreases with GO content. For example, at 0.5 and 0.75 wt%, the porosity percentages were determined as 31% and 28.5%, respectively. A similar observation was reported in our previous work [45] when polyurea/graphene

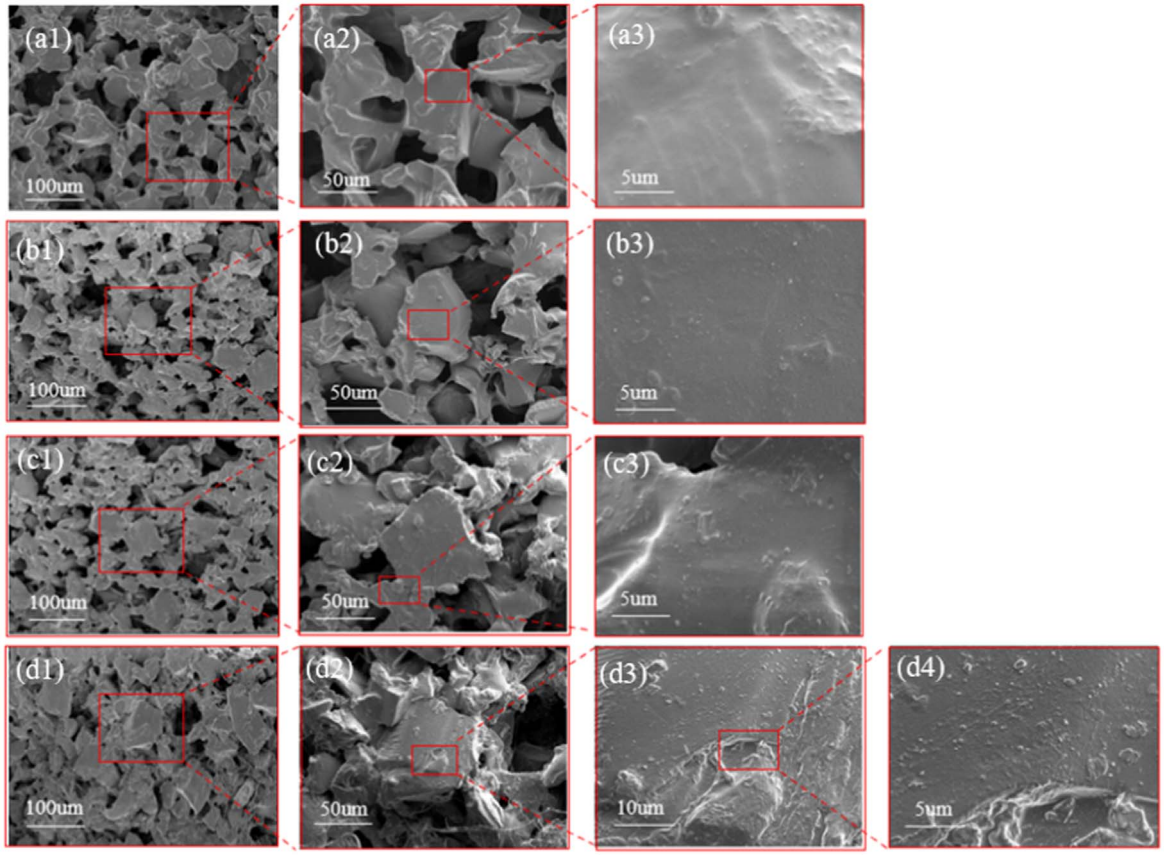

Figure 3. SEM micrographs of neat PVA and its GO composites: (a1)–(a3) neat PVA; (b1)–(b3) 0.25 wt%-based composite; (c1)–(c3) 0.5 wt%-based composite; and (d1)–(d4) 0.75 wt%-based composite.

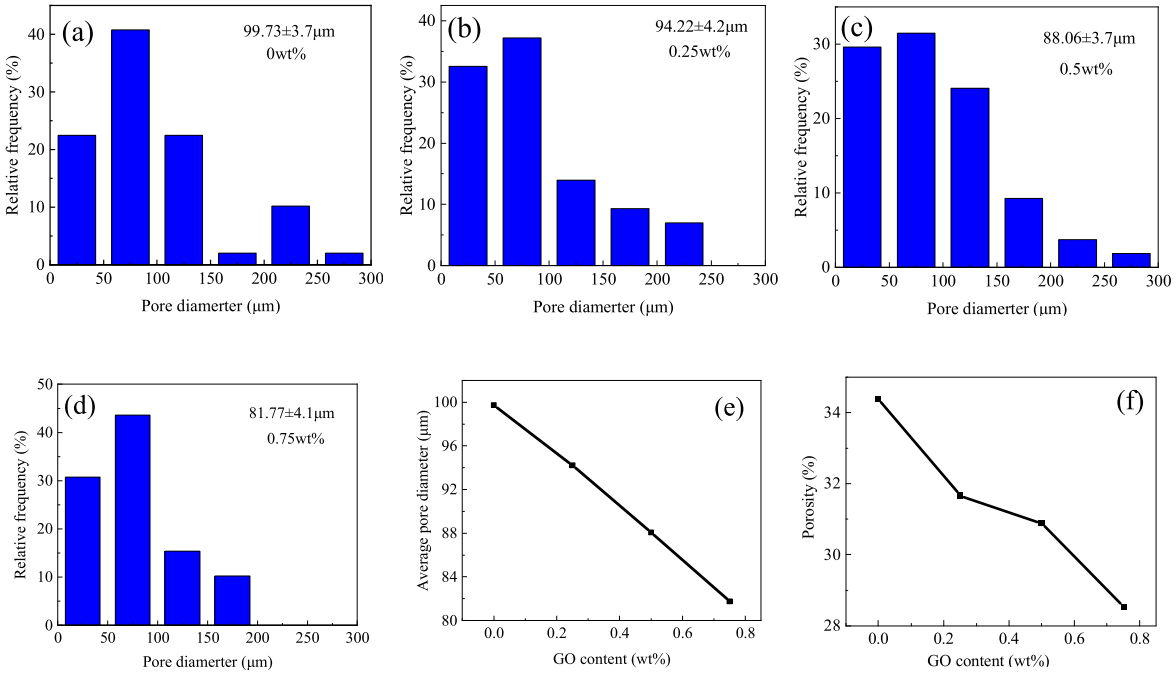

Figure 4. Pore size and porosity analysis of PVA/GO composite films at (a) 0.0 wt%, (b) 0.25 wt%, (c) 0.5 wt%, and (d) 0.75 wt%. (e) Relation between pore size and wt% of GO of PVA composite. (f) Relation between porosity and wt% of GO of PVA composite.

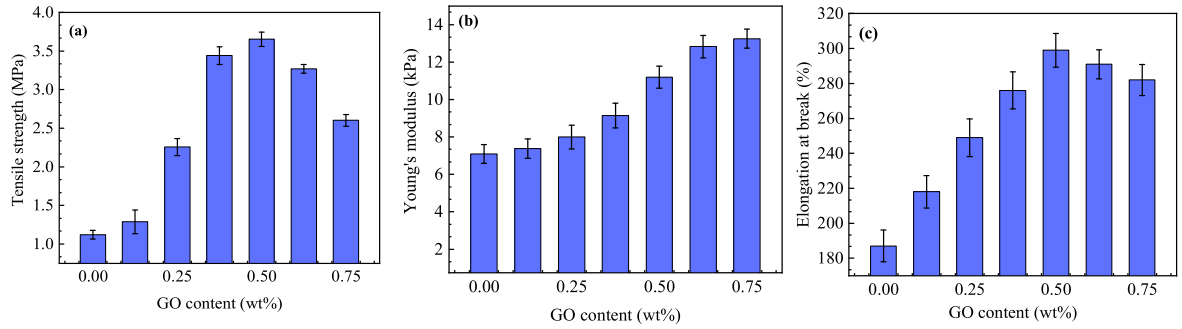

Figure 5. Mechanical properties of porous PVA/GO composite films: (a) tensile strength; (b) Young's modulus; and (c) elongation at break.

platelets were prepared using a dry cast and phase-separation approach; the average diameter of the pores was decreased by 44% and 52% by adding 5 wt% and 8 wt%, respectively, in comparison with neat polyurea. In general, fillers such as GO can work as nucleation sites during the foaming process, thereby making the material less porous.

3.3. Mechanical measurements

Figures 5(a)–(c) show the tensile strength, Young's modulus, and elongation at break of neat PVA and its GO-based composite films. It is evident that adding GO enhances the tensile strength, elongation at break, and Young's modulus of the PVA film. Figure 5(a) shows that the maximum tensile strength of the PVA/GO composite film has reached 3.652 MPa at 0.5 wt%, depicting an increment of 225% as compared to neat PVA film. In figure 5(b), the Young's modulus increased from 7.09 kPa for neat PVA to 13.25 kPa at 0.75 wt%, representing an 86.88% increment. As shown in figure 5(c), when the fraction of GO is 0.5 wt%, the elongation at break of the composite reaches a maximum of 299%, which is 37.16% higher than that of the neat PVA film. This enhancement is due to the fact that GO can provide a larger specific surface area, and its epoxy oxygen-containing group can be combined with PVA through a hydrogen bond, which significantly improves the strength and stiffness of the PVA film. However, the maximum tensile strength and elongation at break at 0.75 wt% are 80% and 6%, respectively, which are lower than those at 0.5 wt%. This may be because of the uneven dispersion and the aggregation of GO platelets, which affect the reinforcing efficiency of GO [45].

Young's modulus is the resistance to deformation of a material in the elastic region where the stiffness of the added filler is dominant. GO causes rigidity enhancement of the PVA chain to restrict the movement of the molecular chains, leading to a high Young's modulus [46, 47]. Tensile strength and elongation at break commonly drop after a certain weight percentage while the Young's modulus continues to rise [48, 49].

3.4. Piezoresistive performance of PVA/GO films

In recent years, flexible sensors have attracted much attention in research because of their wearability, easy multi-functional integration, and biocompatibility [50–52]. In order to investigate the sensing performance of porous PVA/GO, the resistance changes of the PVA/GO composite films under tensile, compression, bending, and twisting loads were examined, as presented in figure 6. First, PVA composite films at 0.25, 0.5, and 0.75 wt% were tested under tensile strain, as shown in figure 6(a); it is evident that 0.5 wt% GO shows the highest sensitivity in comparison to other fractions. Therefore, taking into account the mechanical properties of the 0.5 wt%-based PVA composite along with its sensitivity, we considered using a 0.5 wt% composite for other electro-mechanical measurements.

When the strain range is 0%–100%, the resistance of the composite film linearly increases with the increase in tensile strain recording a gauge factor of 2.46 (246%), as shown in figure 6(b). The increase in electrical resistance upon applying tensile strain follows these sequences: (i) when the composite is subjected to a pulling effect, the connected electrically conductive network becomes disrupted; (ii) thus the distance between the GO plates becomes large; and, ultimately (iii) some of the conductive paths are disconnected, leading to a composite film with high electrical resistance.

Figure 6(c) shows the resistance of the PVA/GO composite film under different compression loads: 0.1 kPa, 0.5 kPa, 1 kPa, 2 kPa, and 5 kPa. As shown in figure 6(c), the resistance gradually decreases with the increase in compressive load. When the maximum pressure increases to 5 kPa, the resistance of the nanocomposite drops to 3.3 kΩ, which is 81% lower than the resistance at a neutral state (0 kPa pressure). The decrease in resistance is due to the porous network structure of the composite film. When a compressive load is applied, the distance between the GO sheets becomes small, forming more conductive paths. Thanks to the porous structure, the sensitivity is significant due to the squeezability of the porous PVA/GO composite. Moreover, the PVA/GO composite can perceive pressure as low as 0.1 kPa, representing high resolution sensitivity for uniform compressive loads.

Sensitivity to compressive loads was further investigated by measuring the response time and recovery time of the PVA/GO composite under 5 kPa; figure 6(d) shows the response and recovery times of the PVA/GO composite at 5 kPa. Both times were almost identical; the response time was 100 msec and the recovery time was 102 msec. The short response and recovery times are due to the porous network structure and elasticity of the composite, and the multitude of

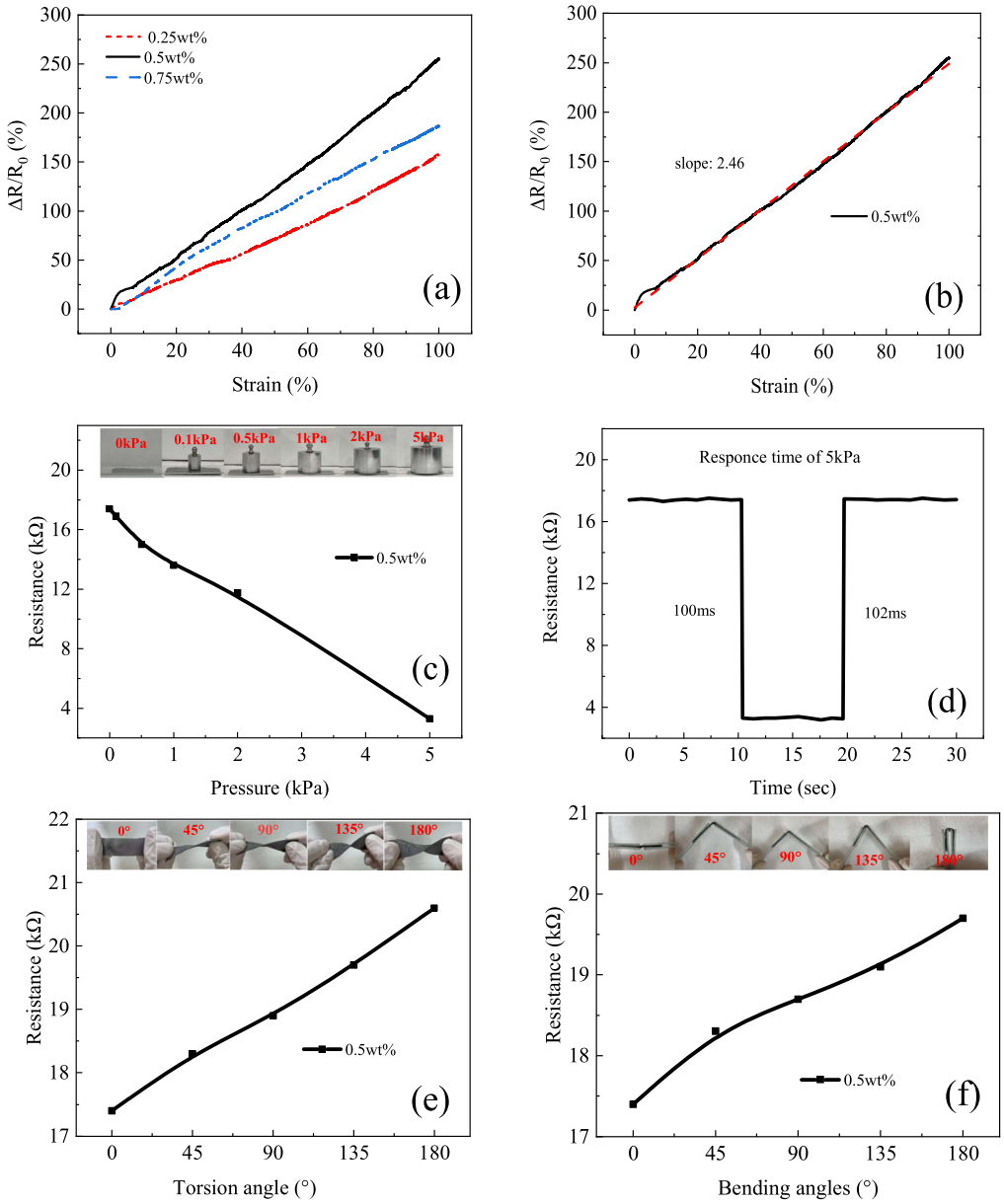

Figure 6. Electromechanical performance of the porous PVA/GO composite film: (a) resistance change versus strain at 0.25, 0.5, and 0.75 wt% of GO; (b) resistance change at 0.5 wt% GO under tensile strain; (c) and (d) electrical resistance of 0.5 wt%-PVA/GO under compressive load and its response time at 5kPa; and (e) and (f) electrical resistance of the PVA/GO composite as a function of torsion and bending angles.

GO sheets at the pore's walls. The sensitivity of the PVA/GO composite was further studied for other mechanical strains, namely bending and twisting strains. Figures 6(e)–(f) show the resistance of the PVA/GO composite under 45°, 90°, 135°, and 180° torsion and bending loads. Under both loads, the resistance linearly increases with the angle. When the torsion and bending angles are increased to 180°, the resistance reaches a maximum of 20.6 and 19.7 kΩ, representing a change of 18.4% and 13.2%, respectively, in comparison with the neutral state. The sensing mechanisms in bending and torsion strains are similar to those in compression and tensile strains.

It is concluded that the PVA/GO composite film is highly sensitive to various mechanical loads including tensile, compression, bending, and torsion loads. Therefore, it is believed that the conductive porous PVA/GO composite has a potential application in structural health monitoring where combined stresses are usually expected.

3.5. Reliability and resilience of the PVA/GO composite strain sensor

Reliability and durability are crucial factors when investigating the properties of strain sensors. Therefore, the PVA composite film at 0.5 wt% of GO was subjected to 0%–10% and 0%–50% tensile strain and 45° and 90° bending at 3.33 Hz for 20 × 103 loading–unloading cycles, as shown in figure 7. Overall, the PVA/GO composite film shows

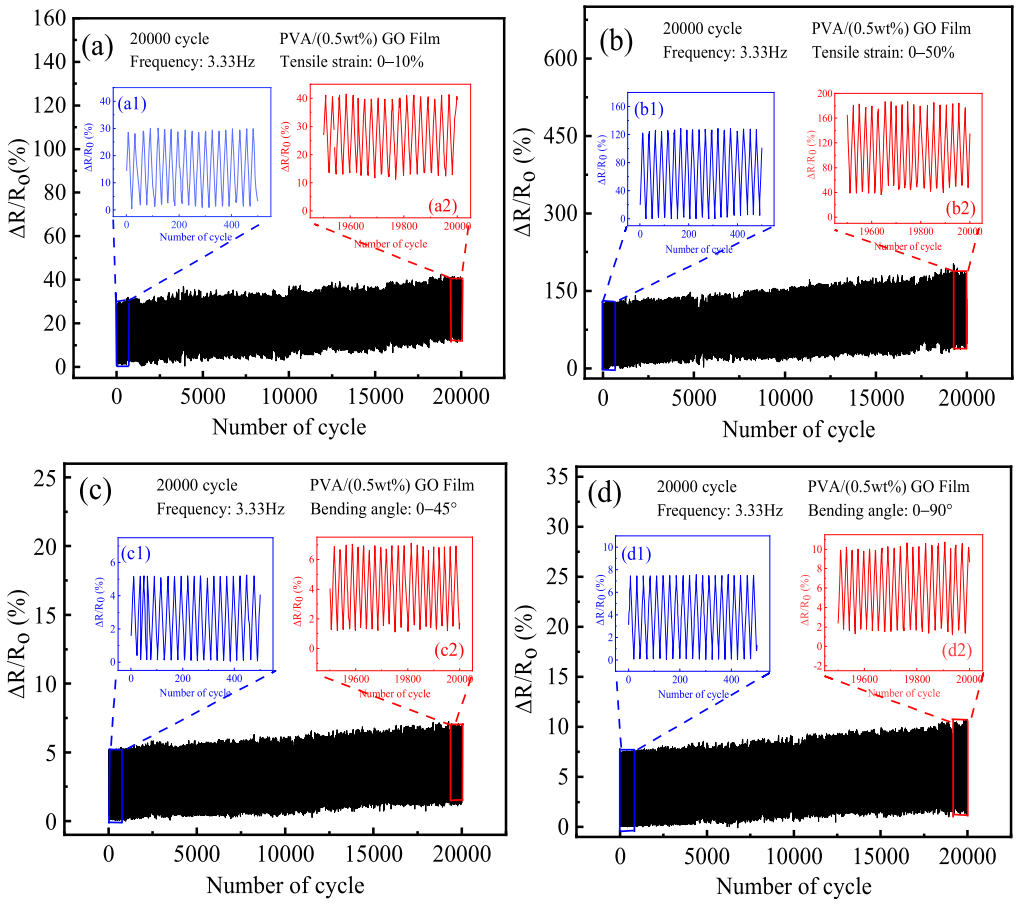

Figure 7. The cyclic test of the porous PVA/GO composite film under 10% and 50% tensile strain and 45° and 90° bending at 3.3 Hz: (a) the cyclic of 10% tensile strain test over 20 000 cycles; (a1)–(a2) magnified images of composite film responses within ranges of 0–500 and 19 500 –20 000 cycles, respectively. (b) The cyclic of 50% tensile strain test over 20 000 cycles; (b1)–(b2) magnified images of composite film responses within ranges of 0–500 and 19 500 –20 000 cycles, respectively. (c) The cyclic of 45° bending test over 20 000 cycles; (c1)–(c2) magnified images of composite film responses within ranges of 0–500 and 19 500 –20 000 cycles, respectively. (d) The cyclic of 90° bending test over 20 000 cycles; (d1)–(d2) magnified images of composite film responses within ranges of 0–500 and 19 500 –20 000 cycles, respectively.

robustness and outstanding reliability over long-term cycling; the change in relative resistance (ΔR/Ro) was between a minimum value of ∼0.47% and a maximum value of 41.1% after 20 × 10^3 loading cycles, as presented in figure 7(a). When the first 500 cycles are magnified (see inset), as in figure 7(a1), the cyclic performance of the sensor is robust, stable, and reliable; the resistance constantly changes within the range of 0.5%–31%. Similarly, the last 500 cycles were magnified (see inset), as in figure 7(a2), indicating that the relative resistance change is between 11.2% and 41.1%. The fluctuation range is similar to the first 500 cycles. However, this represents a 22% and 32% shift in the lower and upper limits of the resistance change between the first and the last 500 cycles.

Furthermore, the PVA/GO composite film was cyclically tested at a higher strain range (0%–50%), as shown in figure 7(b). The change trend of relative resistance in figure 7(b) is similar to that in figure 7(a); the relative resistance changes within the range of 0.02%–186.9% under 0%–50% tensile strain. In the first 500 cycles (inset in figure 7 (b1)), the relative resistance changes between a minimum value of 0.02% and a maximum value of 120% while the relative resistance varies between 40% and 186% in the last 500 cycles, as shown in the inset of figure 7(b2). The previous report [53]—using poly(dimethylsiloxane) as the matrix—shows that the resistance of the composite film changes more under high strain. Despite the PVA composite film having good sensitivity at a high strain range, its internal structure revealed prominent damage at a high strain range (0%–50%) in comparison with a low strain range (0%–10%). The deterioration in the internal structure is expected after such a long period of cyclic loading due to the irreversible damage that occurred in the GO network within the PVA matrix. The internal structural damage is due to two factors, as follows.

(i) Upon loading, the conductive paths of GO are stretched, making the overlap distance small, resulting in high resistance. When the load is released, the GO sheets return to their original sites. Applying low strain will result in spring-like behavior for the GO sheets, depicting constant change in the relative resistance; this means the global network inside the matrix stays connected for a period of time. On the other hand, when a high level of strain is applied over the composite, the

conductive network inside the host polymer rapidly breaks into sub-networks instead of having one global network. These sub-networks have loose contact between each other in comparison to a robust contact when they are in one global network, as in the low strain range scenario.

(ii) Since polymers possess viscoelastic behavior, the host PVA polymer in the PVA/GO composite starts to degrade and experience creep phenomena upon loading and unloading for a long time, for example 20×10^3 cycles. In the first stage of cyclic loading, the host matrix pushes the fillers to their original sites when the load is released—depicting a reversible or spring-like behavior. After a long time of cyclic loading, the polymer chains are not fully recoverable due to creep behavior. Consequently, some of the GO sheets do not return to their original place and are disconnected from the global network of the filler, leading to a permanent change in the structure. Transiting from reversible to partially irreversible behavior depends on the rate and value of the applied strain; faster and higher strain promotes quick irreversible behavior.

Figures 6(c) and (d) show the relative resistance change of the composite film over 20×10^3 cycles within bending ranges of 0°–45° and 0°–90°. When the first 500 cycles are magnified (see inset), as in figure 7(c1), the relative resistance changes within the range of 0.04%–5.25%; the last 500 cycles were magnified (see inset), as in figure 7(c2), depicting a relative resistance change between 1.16% and 7.08%. Figures 7(d1)–(d2) show that the relative resistance changes between 0.1% and 7.46% in the first 500 cycles, and 1.6% and 10.7% in the last 500 cycles. The aforementioned mechanism of internal damage due to loading applies here as well. Although the resistance changes more under high strain, the PVA sensor still has reliability and resilience in practical applications. Therefore, we expect the PVA/GO composite film to have remarkable stability in structural health-monitoring applications.

3.6. Water resistance of the PVA/GO composite film

There are a large number of hydroxyl groups on the molecular chain of PVA. Hydroxyl is a hydrophilic group, so the PVA film has good water absorption and solubility. However, because the PVA film easily uptakes water and swells, resulting in a decline in gas barrier and mechanical properties, it is worthwhile to study water resistance upon adding GO. Therefore, 20 × 20−mm samples of the PVA/GO composite were soaked in deionized water for 25 h, when water absorption is expected to reach a saturation state. Results of water absorption of the PVA/GO composite film are presented in figure 8. At equilibrium, the water-absorption percentage of neat PVA reached 111%. It is clear that adding GO into PVA significantly reduces water uptake; for example, 0.25 wt% GO reduces the water absorption of PVA from 111% to 67%. The water-absorption percentage decreases further with the increase in GO content; at 0.75 wt%, the

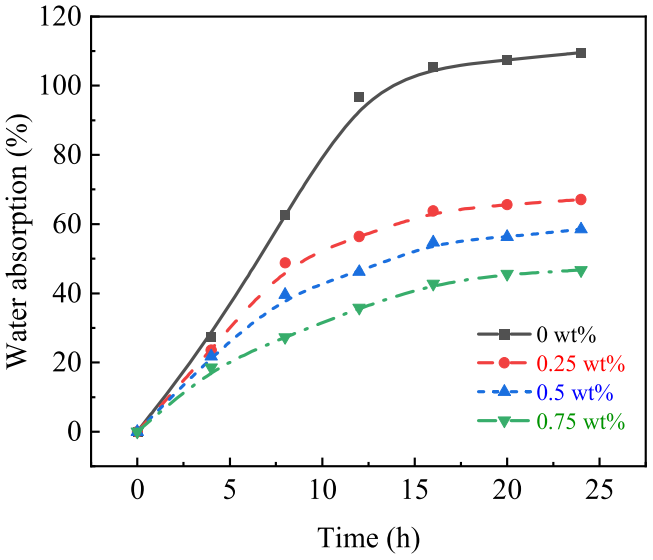

Figure 8. Water absorption of porous PVA/GO composite films.

water absorption was 47%, representing a reduction of 58%. The decrease in water absorption of PVA with the addition of GO is due to two main reasons, as follows. (i) GO has oxygen-containing groups, which can generate hydrogen bonds with PVA. This reduces the number of free hydroxyl groups in the PVA molecular chain. (ii) The nanosize and plate-like structure of GO provide a large specific surface area; the GO layers are mutually overlapped, forming a large mesh structure so that the water molecules penetrate along a tortuous path within the composite.

3.7. The chemical resistance of the PVA/GO composite film

Herein, we investigated the properties of PVA/GO in acidic and alkaline environments. The 0.5 wt% composite film was immersed in 2% sulfuric acid solution and 0.1% sodium hydroxide/calcium hydroxide solution for seven days to assess its acid and alkaline corrosion resistance. The mechanical properties and electromechanical response of the PVA/GO composite film after immersion are recorded in table 1, which shows that the composite film has similar resistance to acid and alkaline solutions.

After soaking in an alkaline solution, the tensile strength and elongation at break of the composite film were 3.26 MPa and 283%, respectively. Moreover, the strain sensitivity was 2.32 (232%) with a response time of 116 msec. When the PVA/GO was soaked in an acidic environment, the mass of the PVA/GO increased by 51.23%; the tensile strength was 3.42 MPa; elongation at break was 283%; the compression response time was 109 msec and the strain sensitivity was 2.37 (237%). The absorption ratio of the 0.5 wt% PVA/GO composite film after immersion in acid and alkaline solutions is shown in figures 9(b)–(c). It is noted that the absorption behavior of the PVA/GO composite film was the same in both environments; the PVA/GO composite film rapidly reached its absorption equilibrium after one day, when the plateau status started. Although the PVA/GO film has good acid and alkali resistance, with the increase of immersion

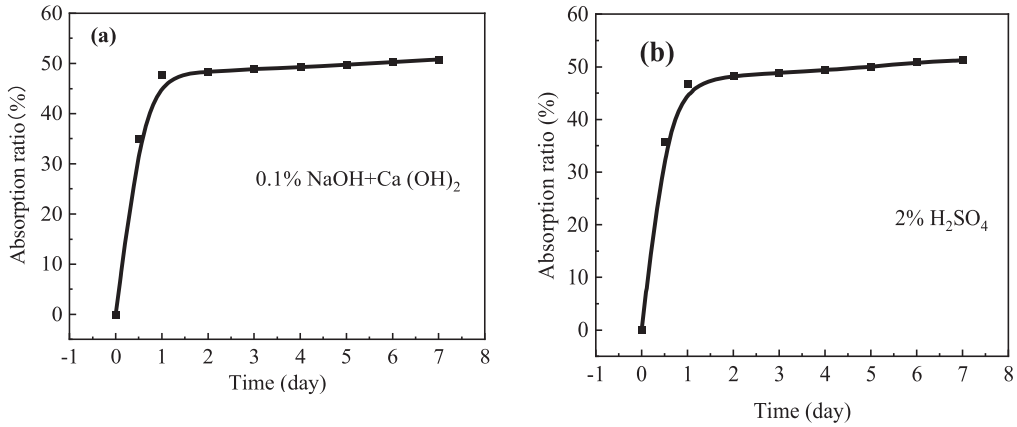

Figure 9. Absorption ratio of the PVA/GO composite film after soaking in two mediums: (a) 0.1%NaOH + Ca $(OH)_2$ and (b) 2% H_2SO_4.

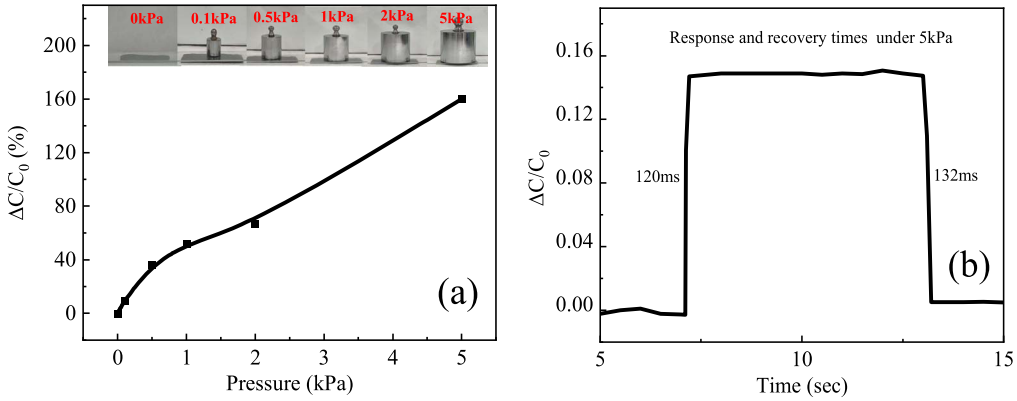

Figure 10. Characteristics of the PVA/GO (0.5 wt%) composite film as a capacitive pressure sensor: (a) capacitance change rate under different pressures; and (b) response and recovery times under 5 kPa.

Table 1. The chemical resistance property of the PVA/GO composite film.

Medium	Tensile strength (MPa)	Elongation @ break(%)	Weight gain(%)	Response time (msec) @ 5kPa	Gauge factor
Air medium	3.652	299	0	100	2.46
2% H_2SO_4	3.428	283	51.23	109	2.37
0.1%NaOH + Ca $(OH)_2$	3.26	270	50.8	116	2.32

time, the internal structure of the film will still be damaged; therefore, the water resistance will decline and the time to reach swelling saturation will become longer. Consequently, the time to reach the saturation point is different between the water-resistance test and the chemical resistance test. Overall, the mechanical properties and electromechanical response of the porous composite film in acidic and alkaline environments were marginally affected, indicating high corrosion resistance and property stability.

3.8. Capacitance performance under different loads

The PVA/GO composite film has the potential to be employed as a capacitive strain sensor due to its porous structure. Figure 10(a) shows the capacitance change rate of a 0.5 wt%-PVA/GO composite under compression stress within the range of 0–5 kPa. It is evident that the relative capacitance of the composite film increases with the increase in compression load; it reaches 161% at 5 kPa. The increase in capacitance is due to the decrease in layer-to-layer distance between GO layers when the composite film is subjected to a compressive load. This leads to an increase in the number of conductive paths as well as capacitance. Figure 10(b) shows the response and recovery times of the PVA/GO composite film under compressive stress of 5 kPa; it recorded 120 and 132 msec, respectively. In a previous study [45], polyurea/graphene platelets (5 wt%) showed a change in relative capacity of 22% upon applying 5 kPa. The results indicate that the porous PVA/GO composite film has high sensitivity as a capacitive pressure sensor.

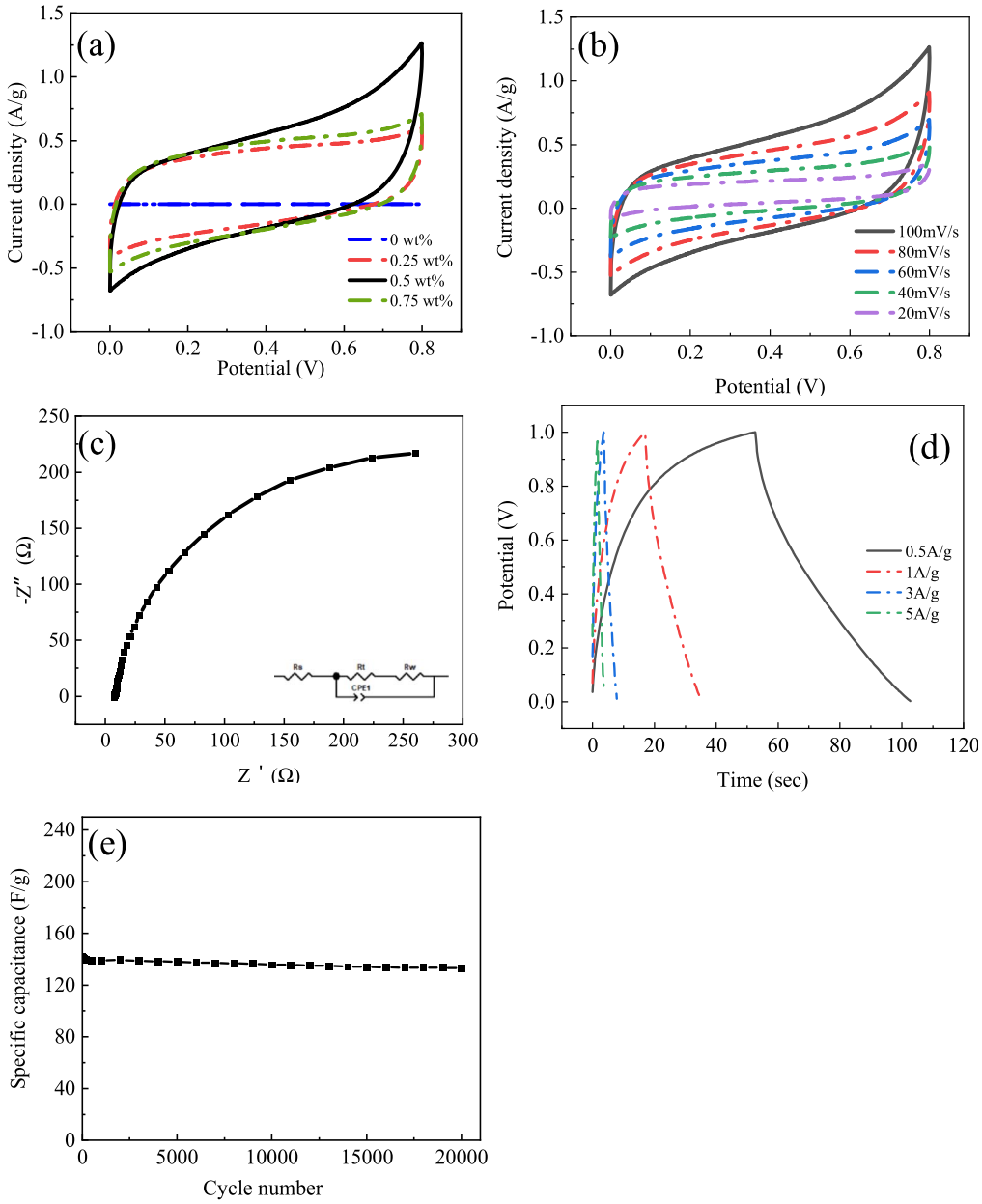

Figure 11. Electrochemical characterization of the porous PVA composite film: (a) CV curves as a function of GO at a scan rate of 100 mV s^{-1}; (b) CV curves at different scanning rates at 0.5 wt% GO; (c) Nyquist diagram of 0.5 wt%-PVA/GO; (d) galvanostatic charge–discharge (GCD) curves of 0.5 wt%-PVA/GO; and (e) stability over 20 × 10^3 cycles.

3.9. Capacitive performance

The porous network structure and excellent electrical conductivity of PVA/GO increase its internal specific surface area and electrically conductive paths. This enhances its electric charge transport kinetics. The electrochemical performance of the PVA/GO composite film was investigated by cyclic voltammetry (CV), galvanostatic charge–discharge (GCD), and electrical impedance spectroscopy (EIS). Figure 11(a) shows the CV curves of the composite film within a potential range of 0–0.8 V. Neat PVA did not show any electrochemical capacitance. On the contrary, the CV curve of the PVA/GO composite film-assembled capacitor maintains a rectangular shape; this shows the characteristics of electrochemical double-layer capacitance behavior, and has an ideal capacitance performance attributable to its high porosity, conductivity, and great mechanical strength. The calculated specific capacitances were 19.3, 25 and 20.2 F g^{-1} when the GO content was 0.25, 0.5 and 0.75 wt%, respectively. This indicates that 0.5 wt% of GO is the optimum content to achieve the highest electrochemical performance.

Figure 11(b) shows CV curves of PVA/GO at 0.5 wt% at a scan rate range of 20–100 mV s^{-1}; all CV curves exhibit a rectangular-like pattern depicting an ideal capacitive behavior and fast charge–discharge performance. This indicates that electron transfer was not confined during the accumulation of charged ions on the surface of the electrode.

Furthermore, the resistance and capacitance characteristics of the electrode were studied by electrochemical

impedance spectroscopy. Figure 11(c) shows the Nyquist plots of the PVA/GO (0.5 wt%) composite film. In general, the Nyquist plots of supercapacitors are comprised of a semicircle in the high-frequency region and an approximately vertical line in the low-frequency region [54]. The semicircle at high frequency reflects the charge-transfer process at the interface; its diameter is related to the charge transfer resistance between the electrode material and the electrolyte. The faster the charge transfer in the charge–discharge process, the more obvious the semicircular curve at high frequency. The ion diffusion resistance of the porous composite film electrode was measured at 40.2Ω.

Figure 11(d) shows the GCD curves of the PVA/GO composite film at various current densities. The specific capacitance was calculated as 119.3, 60.2, 42.8, and 27.5 F g^{-1}, respectively, corresponding to current densities of 0.5, 1, 3, and 5 A g^{-1}. Obviously, the specific capacitance decreases with the increase in current density due to the changes of ion diffusions with time; the diffusion for a long time can only be achieved at a low current density.

The cycling capacity of the PVA/GO film electrode in electrolyte was measured within a potential range of 0–0.8 V and a current density of 0.5 A g^{-1}. It is evident that the specific capacitance of the synthesized film is stable without significant deterioration over 20 × 10^3 cycles, as shown in figure 11(e) (record data every 1000 cycles). The capacity of the supercapacitor remains above 94.45% of the initial value, showing excellent cycle stability. The electrochemical results of PVA/GO showed it possesses a high specific capacitance and an outstanding cycling stability. These findings designate the PVA/GO composite as a promising electrode material for high-performance capacitors.

4. Conclusions

In this work, a multifunctional, biodegradable, and highly flexible PVA/GO composite film was prepared and investigated. The morphology and structural-property relations were studied. At 0.5 wt% GO, the PVA composite film reached a maximum tensile strength of 3.65 MPa and an elongation at break of 299%. The PVA/GO composite film showed high sensitivity to various mechanical strains including tensile, compressive, bending, and twisting. For example, the sensitivity factor (gauge factor) was recorded as 246% when tensile strain was applied to a 0.5 wt%-based PVA/GO composite film. The composite film was rapid in responding to compressive load; response and recovery times were recorded at 100 msec and 102 msec, respectively.

The PVA/GO composite film endured cyclic loading as a strain sensor over 20 × 10^3 cycles at tensile strain ranges of 0%–10% and 0%–50%; it was also tested under cyclic bending loading for the same number of cycles. It is noteworthy to mention that the PVA/GO experienced 22% and 32% shifts in the lower and upper limits of the resistance change between the first and the last 500 cycles upon loading within the strain range 0%–10%.

Moreover, due to the porous structure of PVA/GO, the film showed enhancements in electrochemical properties; the specific capacitance was 25 F g^{-1} at 0.5 wt% GO. The CV curves of the 0.5 wt%-PVA/GO composite film exhibited a rectangular-like pattern, presenting an ideal capacitive performance and fast charge–discharge behavior. The current study explored an eco-friendly graphene-based polymeric composite for energy storage and structural health-monitoring applications.

Acknowledgments

This work was financially supported by the National Natural Science Foundation (52173077 and 51973123), the China Postdoctoral Science Foundation (2019M651151), the Scientific Research Funds from Liaoning Education Department (LJKZ0187 and JYT2020007), the plan of rejuvenating the talents of Liaoning province (XLYC1907135), and a Social Policy Grant, Nazarbayev University.

Data availability statement

The data that support the findings of this study are available upon reasonable request from the authors.

Declaration

The authors declare no competing financial interests.

ORCID iDs

Sherif Araby https://orcid.org/0000-0001-6807-7926
Fethi Abbassi https://orcid.org/0000-0001-7530-2116
Qingshi Meng https://orcid.org/0000-0002-8187-7028

References

[1] Han S *et al* 2019 A comparative study of two graphene based elastomeric composite sensors *Polym. Test.* **80** 106106
[2] Nishide H and Oyaizu K 2008 Toward flexible batteries *Science* **319** 5864
[3] Shi G *et al* 2016 Highly sensitive, wearable, durable strain sensors and stretchable conductors using graphene/silicon rubber composites *Adv. Funct. Mater.* **26** 42
[4] Gong T *et al* 2018 Highly responsive flexible strain sensor using polystyrene nanoparticle doped reduced graphene oxide for human health monitoring *Carbon* **140** 286–95
[5] Liu H *et al* 2017 Paper: a promising material for human-friendly functional wearable electronics *Materials Science & Engineering R.* **112** 1–22
[6] Wu Q, Xu Y, Yao Z, Liu A and Shi G 2010 Supercapacitors based on flexible graphene/polyaniline nanofiber composite films *ACS Nano.* **4** 1963–70

[7] Khalid M A U and Chang S H 2022 Flexible strain sensors for wearable applications fabricated using novel functional nanocomposites: a review *Compos. Struct.* **284** 115214

[8] Wang G *et al* 2018 Structure dependent properties of carbon nanomaterials enabled fiber sensors for *in situ* monitoring of composites *Compos. Struct.* **195** 36–44

[9] Xu C, Zheng Z, Lin M, Shen Q, Wang X, Lin B and Fu L 2020 Strengthened, antibacterial and conductive flexible film for humidity and strain sensor *ACS Appl. Mater. Interfaces* **12** 35482–92

[10] Peng W W *et al* 2022 Flexible organohydrogel ionic skin with Ultra-Low temperature freezing resistance and Ultra-Durable moisture retention *J. Colloid Interface Sci.* **608** 396–404

[11] Slater A G and Cooper A I 2015 Porous materials. function-led design of new porous materials *Science* **348** aaa8075

[12] Li Y, Fu Z Y and Su B L 2012 Hierarchically structured porous materials for energy conversion and storage *Adv. Funct. Mater.* **22** 22

[13] Lin P *et al* 2016 Synthesis of porous polyurea monoliths assisted by centrifugation as adsorbents for water purification *Colloids Surf., A* **506** 87–95

[14] Nugent P *et al* 2013 Porous materials with optimal adsorption thermodynamics and kinetics for CO_2 separation *Nature: International Weekly Journal of Science.* **495** 7439

[15] Zhang J Q *et al* 2019 Highly stretchable and self-healable MXene/Polyvinyl alcohol hydrogel electrode for wearable capacitive electronic skin *Adv. Electron. Mater.* **5** 7

[16] Liu J *et al* 2017 Magnetic, electrically conductive and lightweight graphene/iron pentacarbonyl porous films enhanced with chitosan for highly efficient broadband electromagnetic interference shielding *Compos. Sci. Technol.* **151** 71–8

[17] Molla-Abbasi P, Ghaffarian S R and Danesh E 2011 Porous carbon nanotube/PMMA conductive composites as a sensitive layer in vapor sensors *Smart Mater. Struct.* **20** 105012

[18] Han L *et al* 2020 A flexible, high-voltage and safe zwitterionic natural polymer hydrogel electrolyte for high-energy-density zinc-ion hybrid supercapacitor *Chem. Eng. J.* **392** 123733

[19] Yu Y L *et al* 2014 Porous carbon nanotube/polyvinylidene fluoride composite material: Superhydrophobicity/superoleophilicity and tunability of electrical conductivity *Polymer* **55** 5616–22

[20] Xu X T *et al* 2017 Three-dimensional networked metal-organic frameworks with conductive polypyrrole tubes for flexible supercapacitors *ACS Appl. Mater. Interfaces* **9** 38737–44

[21] Qin Y *et al* 2018 Effects of organic modification of montmorillonite on the properties of hydroxypropyl Di-starch phosphate films prepared by extrusion blowing *Materials.* **11** 7

[22] Tokiwa Y *et al* 2009 Biodegradability of plastics *Int. J. Mol. Sci.* **10** 3722–42

[23] Yan S *et al* 2014 Unveiling the environment-dependent mechanical properties of porous polypropylene separators *Polymer* **55** 24

[24] Ferreira A D B L, Nóvoa P R O and Marques A T 2016 Multifunctional Material Systems: A state-of-the-art review *Compos. Struct.* **151** 3–35

[25] Dudchenko A V *et al* 2014 Organic fouling inhibition on electrically conducting carbon nanotube–polyvinyl alcohol composite ultrafiltration membranes *J. Membr. Sci.* **468** 1–10

[26] Rathod S G *et al* 2016 High mechanical and pressure sensitive dielectric properties of graphene oxide doped PVA nanocomposites *RSC Adv.* **6** 77977–86

[27] Theophile N and Jeong H K 2017 Electrochemical properties of poly(vinyl alcohol) and graphene oxide composite for supercapacitor applications *Chem. Phys. Lett.* **669** 125–9

[28] Choi H, Nguyen P T and In J B 2019 Laser transmission welding and surface modification of graphene film for flexible supercapacitor applications *Appl. Surf. Sci.* **483** 481–8

[29] Debnath D *et al* 2020 Radio frequency heating and reduction of graphene oxide and graphene oxide - polyvinyl alcohol composites *Carbon* **169** 475–81

[30] Meng Q *et al* 2014 Processable 3 nm thick graphene platelets of high electrical conductivity and their epoxy composites *Nanotechnology* **25** 12

[31] Ren J *et al* 2017 Environmentally-friendly conductive cotton fabric as flexible strain sensor based on hot press reduced graphene oxide *Carbon* **111** 622–30

[32] Wang M *et al* 2021 High-sensitive flexural sensors for health monitoring of composite materials using embedded carbon nanotube (CNT) buckypaper *Compos. Struct.* **261** 113280

[33] Huang Y F, Zhang M Q and Ruan W H 2014 High-water-content graphene oxide/polyvinyl alcohol hydrogel with excellent mechanical properties *J. Mater. Chem. A* **2** 10508–15

[34] Karthikeyan B, Udayabhaskar R and Hariharan S 2016 Tuning optical and three photon absorption properties in graphene oxide-polyvinyl alcohol free standing films *Appl. Phys. Lett.* **109** 2

[35] Layek R K *et al* 2014 Layer-structured graphene oxide/polyvinyl alcohol nanocomposites: dramatic enhancement of hydrogen gas barrier properties *J. Mater. Chem. A* **2** 12158–61

[36] Guo X *et al* 2020 Scalable, flexible and reusable graphene oxide-functionalized electrospun nanofibrous membrane for solar photothermal desalination *Desalination* **488** 114535

[37] Yanji Z *et al* 2015 Nanoindentation and thermal study of polyvinylalcohol/graphene oxide nanocomposite film through organic/inorganic assembly *Appl. Surf. Sci.* **349** 27–34

[38] Kim S, Shimazu J, Fukaminato T, Ogata T and Kurihara S 2017 Thermal conductivity of graphene oxide-enhanced polyvinyl alcohol composites depending on molecular interaction *Polymer* **129** 201–6

[39] Hummers W S and Offeman R E 1958 Preparation of graphitic oxide *JACS* **80** 1339

[40] Kim B H *et al* 2012 Thermally modulated multilayered graphene oxide for hydrogen storage *Phys. Chem. Chem. Phys.* **14** 1480–4

[41] Kovtyukhova N I *et al* 1999 Layer-by-layer assembly of ultrathin composite films from micron-sized graphite oxide sheets and polycations *Chem. Mater.* **11** 771–8

[42] Yang Z *et al* 2019 High-mass loading electrodes with exceptional areal capacitance and cycling performance through a hierarchical network of MnO2 nanoflakes and conducting polymer gel *J. Power Sources* **412** 655–63

[43] Boukhvalov D W *et al* 2018 Atomic and electronic structure of graphene oxide/Cu interface *Thin Solid Films* **665** 99–108

[44] Gomez J, Villaro E, Karagiannidis P G and Elmarakbi A 2020 Effects of chemical structure and morphology of graphene-related materials (GRMs) on melt processing and properties of GRM/polyamide-6 nanocomposites *Results in Materials* **7** 100105

[45] Cui X *et al* 2022 Multifunctional, flexible and mechanically resilient porous polyurea/graphene composite film *J. Ind. Eng. Chem.* **105** 549–62

[46] Cui X *et al* 2020 Multifunctional graphene-based composite sponge *Sensors* **20** 2

[47] Meng Q *et al* 2020 Multifunctional, durable and highly conductive graphene/sponge nanocomposites *Nanotechnology* **31** 46

[48] Wang S *et al* 2021 Thermal conductivity and mechanical performance of hexagonal boron nitride nanosheets-based epoxy adhesives *Nanotechnology* **32** 355707

[49] Han S *et al* 2019 Mechanical, toughness and thermal properties of 2D material- reinforced epoxy composites *Polymer* **184** 121884
[50] Meng Q *et al* 2020 A highly flexible, electrically conductive, and mechanically robust graphene/epoxy composite film for its self-damage detection. *J. Appl. Polym. Sci.* **137** 34
[51] Wang Y *et al* 2014 Wearable and highly sensitive graphene strain sensors for human motion monitoring *Adv. Funct. Mater.* **24** 29
[52] Fu Y F, Li Y Q, Liu Y F, Huang P, Hu N and Fu S Y 2018 High performance structural flexible strain sensor based on graphene coated glass fabric/silicone composite *ACS Applied Materials & Interfaces* **10** 35503–9
[53] Zhang F *et al* 2021 3D interconnected conductive graphite nanoplatelet welded carbon nanotube networks for stretchable conductors *Adv. Funct. Mater.* **31** 2107082
[54] Wang Y *et al* 2009 Supercapacitor devices based on graphene materials *J. Phys. Chem. C* **113** 13103–7